Chapter 3

Characterization of heralded entanglement between two atomic ensembles

This chapter is largely based on ref. [34]. Reference [34] refers to the then current literature in 2007 at the time of publication.

3.1 Introduction

Beyond a fundamental significance, quantum control of entanglement between material systems is an essential capability for quantum networks and scalable quantum communication architectures (refs. [9,162], see also chapter 1). In recent years, significant advances have been achieved in the control of the quantum states of atomic systems, including entanglement of trapped ions [197,198] and between macroscopic spins [59]. By following the seminal paper of Duan, Lukin, Cirac, and Zoller (*DLCZ*) (ref. [4], chapter 2), entanglement between single collective excitations stored in two remote atomic ensembles has also been demonstrated [27]. In the *DLCZ* protocol, entanglement is created in a probabilistic but heralded way from quantum interference in the measurement process [199–201]. The detection of a photon from one or the other atomic ensemble in an indistinguishable fashion results in an entangled state with one collective spin excitation shared coherently between the ensembles[a]. Such entanglement has been critical for the initial implementation of functional quantum nodes for entanglement distribution (ref. [36], chapter 4), for the investigation of entanglement swapping (ref. [37], chapter 5) and for light-matter teleportation [112].

Because of the relevance to quantum networking tasks, it is important to obtain detailed characterizations of the physical processes related to the creation, storage, and utilization of heralded entanglement. Towards this end, significant advances have been demonstrated in the generation of photon-pairs [74,75] and the efficient retrieval of collective excitation [76,77]. Moreover, decoherence processes for a single atomic ensemble in the

[a] See also chapter 9 for an initial demonstration of measurement-induced entanglement of spin waves among multiple quantum memories.

regime of collective excitation have been investigated theoretically (ref. [147], chapter 2) and a direct measurement of decoherence for one stored component of a Bell state recently was performed [202]. However, to date no direct study has been reported for the decoherence of an entangled system involving two distinct atomic ensembles, which is a critical aspect for the implementation of elaborate protocols [122,123,203]. The decoherence of entanglement between ensembles has been shown in recent setups (chapter 2), through the decay of the violation of a Bell inequality (ref. [36], chapter 4) and the decay of the fidelity of a teleported state [112]. However, a quantitative analysis was not provided since these setups involved many other parameters, such as phase stability over long distances.

In this chapter, I discuss measurements that provide a detailed and quantitative characterization of entanglement between collective atomic excitations. Specifically, we determine the concurrence C (ref. [178]) as a function of the normalized degree of correlation g_{12} (ref. [76]) for the ensembles, including the threshold $g_{12}^{(0)}$ for entanglement ($C > 0$). We also map the decay of the concurrence $C(\tau)$ as a function of storage time for the entangled state, and interpret this decay by measuring the local decoherence on both ensembles taken independently. Compared to ref. [27], these observations are made possible by a new system that requires no active phase stability and that implements conditional control for the generation, storage, and readout of entangled atomic states.

3.2 Experimental setup

Our experiment is illustrated in Fig. 3.1. A single cloud of cesium atoms in a magneto-optical trap is used; two ensembles are defined by different optical paths 1 mm apart [36,204]. This separation is obtained by the use of birefringent crystals close to the cloud, which separate orthogonal polarizations [71]. At 40 Hz, the trap magnetic field is switched off for 7 ms. After waiting 3 ms for the magnetic field to decay, the two samples are simultaneously illuminated with 30-ns-long and 10 MHz red-detuned write pulses, at a rate of 1.7 MHz. Given the duty cycle of the experiment, the effective rate is 180 kHz. Spontaneous Raman scattered fields induced by the write beams are collected into single-mode fibers, defining for each ensemble optical modes that we designate as fields $1_{U,D}$ with 50 μm waist and a 3° angle relative to the direction of the write beams [75,76]. The fields $1_{U,D}$ are frequency filtered to block spontaneous emission from atomic transitions $|e\rangle \rightarrow |g\rangle$, which do not herald the creation of a collective excitation. After this stage, and before detection, fields $1_{U,D}$ are brought to interfere on a polarizing beam-splitter. A detection event at $D_{1a,1b}$ that arises indistinguishably from either of the fields $1_{U,D}$ projects the atomic ensembles into an entangled state where, in the ideal case, one collective excitation is coherently shared between the U, D ensembles [4,27].

3.3 Entanglement generation and storage

In the ideal case of small excitation probability, the atom-field 1 joint state can be written for each ensemble:

$$|\Psi\rangle = |0_a\rangle|0_1\rangle + \sqrt{\xi}|1_a\rangle|1_1\rangle + O(\xi) \ , \tag{3.1}$$

with $|n_1\rangle$ the state of the field 1 with n photons and $|n_a\rangle$ the state of the ensemble with n collective excitations (chapter 2). Upon a detection event at $D_{1a,1b}$, in the ideal case, the atomic state is projected into

$$|\Psi_{U,D}\rangle = \frac{1}{\sqrt{2}}(|0_a\rangle_U|1_a\rangle_D \pm e^{i\phi}|1_a\rangle_U|0_a\rangle_D) + O(\sqrt{\xi}), \tag{3.2}$$

where $|0_a\rangle_{U,D}, |1_a\rangle_{U,D}$ refers to the two ensembles U, D with $0, 1$ collective excitations, respectively[4]. The $\pm$ sign is set by the detector that records the heralding event. The overall phase ϕ is the sum of the phase difference of the write beams at the U and D ensembles and the phase difference acquired by fields 1 in propagation from the ensembles to the beamsplitter. To achieve entanglement, this phase must be constant from trial to trial[110]. In order to meet this requirement, the initial demonstration reported in ref.[27] employed

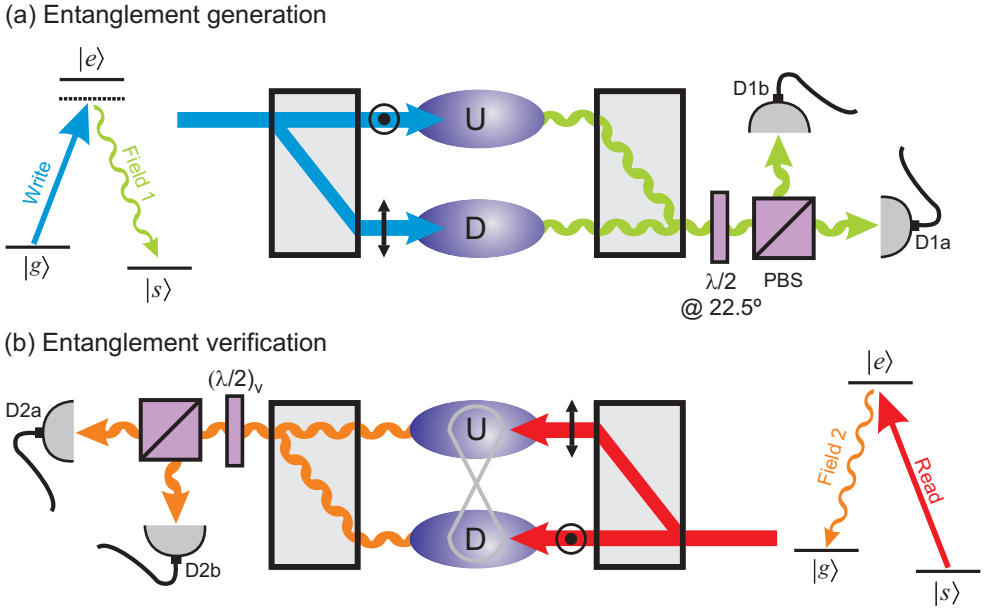

Figure 3.1: **Entanglement generation and verification.** **a**, Entanglement generation and storage. A weak write pulse is split into two paths separated by 1 mm and excites simultaneously two atomic samples, U, D. The resulting fields $1_{U,D}$ are combined at the polarizing beamsplitter (PBS) and sent to the single-photon detectors $D_{1a,1b}$. A detection event at D_{1a} or D_{1b} heralds the creation of entanglement. **b**, Entanglement verification. After a storage time τ, entanglement is verified by mapping the atomic state to propagating fields $2_{U,D}$ by way of read pulses. Tomography is then achieved in two steps, as described in the text. The atomic cloud is initially prepared in the ground state $|g\rangle$. $\{|g\rangle, |s\rangle, |e\rangle\}$ denote the levels $\{|6S_{1/2}, F = 4\rangle, |6S_{1/2}, F = 3\rangle, |6P_{3/2}, F = 4\rangle\}$. Note that the fields $1_{U,D}$ and $2_{U,D}$ are detected with a small angle relative to the classical beams, which is not represented here for the sake of simplicity.

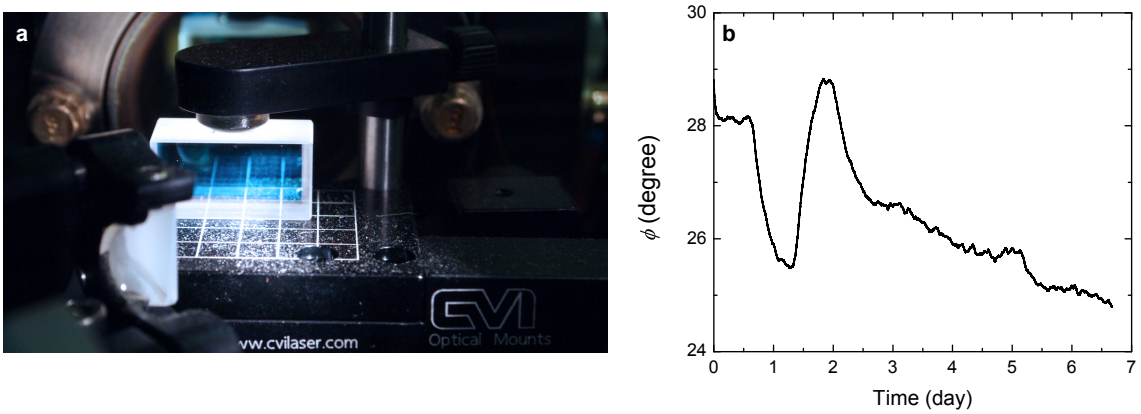

Figure 3.2: **Passive stability of a Mach-Zehnder interferometer formed by a pair of beam displacers. a**, A calcite beam displacer mounted on a stable prism mount. **b**, Long-term phase instability of an interferometer formed by two beam displacers. By mounting the two crystals in an anti-symmetric configuration (Fig. 3.1), the phase drifts are passively compensated to the first order for thermal expansions of the crystals as well as for mechanical instabilities along all translational degrees of freedom (except for tilting). The relative phase ϕ does not change by more than a few degrees over several days.

auxiliary fields to achieve active stabilization for various phases for two ensembles located in distinct vacuum apparatuses. By contrast, in our current setup (Fig. 3.1a), ϕ is determined only by the differential phase for the two paths with orthogonal polarizations defined by the birefringent crystals (Fig. 3.2a); our small setup has sufficient passive stability without the need of adjustment or compensation. The relative phase ϕ does not change by more than a few degrees over 24 hours (Fig. 3.2b).

3.4 Entanglement verification

To operationally verify entanglement between the U, D ensembles, the respective atomic states are mapped into photonic states by applying simultaneously read pulses in the configuration introduced in ref.[75], as depicted in Figure 3.1b (see also chapter 5.3.3). The delocalized atomic excitation is retrieved with high efficiency thanks to collective enhancement[4,76] and, in the ideal case, $|\Psi_{U,D}\rangle$ would be mapped directly to the photonic state of fields $2_{U,D}$ with unity efficiency and no additional components. Stability for the phase difference of the read beams and of fields $2_{U,D}$ is also required in this process; it is again achieved by the passive stability of our current scheme[71]. Since entanglement cannot be increased by local operations[205], the entanglement for the atomic state will always be greater than or equal to that measured for the light fields.

A model-independent determination of entanglement based upon quantum tomography of the fields $2_{U,D}$ has been developed in ref.[27]. The model consists of reconstructing a density matrix, $\tilde{\rho}_{2_U,2_D}$, obtained from the full density matrix by restriction to the subspace with no more than one photon per mode. We also assume that all off-diagonal elements between states with different numbers of photons vanish. The model thus leads to a lower bound for entanglement. As detailed in ref.[27], $\tilde{\rho}_{2_U,2_D}$ can be written in the photon-number basis

$|n\rangle|m\rangle$ with $\{n,m\}=\{0,1\}$ as follows:

$$\tilde{\rho}_{2_U,2_D}=\frac{1}{P}\begin{pmatrix} p_{00} & 0 & 0 & 0 \\ 0 & p_{01} & d & 0 \\ 0 & d^* & p_{10} & 0 \\ 0 & 0 & 0 & p_{11} \end{pmatrix}. \tag{3.3}$$

Here, p_{ij} is the probability to find i photons in mode 2_U and j in mode 2_D; d is the coherence term between the $|1\rangle|0\rangle$ and $|0\rangle|1\rangle$ states; and $P=p_{00}+p_{01}+p_{10}+p_{11}$. From $\tilde{\rho}_{2_U,2_D}$, one can calculate the concurrence C, which is a convenient monotone measurement of entanglement ranging from 0 for a separable state to 1 for a maximally entangled state[178]:

$$C=\max(0,C_0) \text{ with } C_0=\frac{1}{P}(2|d|-2\sqrt{p_{00}p_{11}}). \tag{3.4}$$

In the regime of low excitation and detection probabilities in which the experiment is performed, the vacuum p_{00} can be approximated by $p_{00}\sim 1-p_c$, while the terms p_{01} and p_{10} are given by $p_{10}=p_{01}=p_c/2$. p_c is the conditional probability of detecting a photon in field 2 from one ensemble following a detection event for field 1.

Experimentally, we reconstruct $\tilde{\rho}_{2_U,2_D}$ and then calculate C by using two configurations for the detection of fields $2_{U,D}$, corresponding to two settings of the $(\lambda/2)_v$ waveplate shown in Fig. 3.1b. The diagonal elements of $\tilde{\rho}_{2_U,2_D}$ are determined from measurements of the photon statistics for the separated fields $2_U, 2_D$, i.e., by detecting independently each field. To access the coherence term d, fields $2_{U,D}$ are coherently superimposed and the count rates from the resulting interference are recorded as a function of the relative phase between the $2_{U,D}$ fields. It can be shown that $d\simeq V(p_{10}+p_{01})/2\sim Vp_c/2$ (ref.[27]), where V is the visibility of the interference fringe.

3.5 Main results

3.5.1 Scaling behavior of heralded entanglement to excitation probability

To investigate the scaling of entanglement with excitation probability ξ, we determine the concurrence C for various values of ξ for fixed memory time $\tau=200$ ns. As ξ increases, higher-order terms in the expansion of Eq. (3.2) cannot be neglected, precisely as in parametric down-conversion. A convenient parameter to assess the excitation regime of each ensemble is the normalized intensity cross-correlation function g_{12} between field 1 and field 2 (ref.[76]), defined as $g_{12}=p_{12}/(p_1p_2)$ with p_{12} the joint probability for detection events from field 1 and 2 in a given trial and p_i the probability for unconditional detections in field i. In the ideal case, this function is related to the excitation probability ξ by $g_{12}=1+1/\xi$, where $g_{12}>2$ defines the

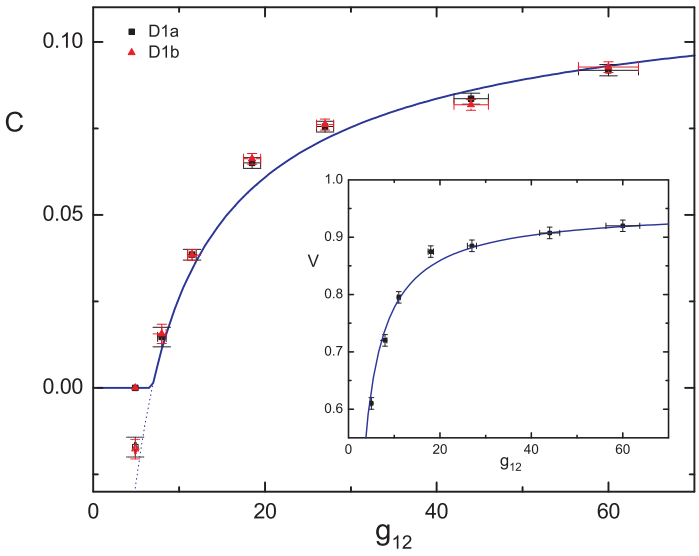

Figure 3.3: **Concurrence C as a function of the normalized cross-correlation function g_{12}, for the two possible heralding events (detection at D_{1a} or D_{1b}).** The solid line is obtained from Eq. (3.5) with the fitted overlap (see inset) and taking an independently-measured retrieval efficiency at 13.5%. The dotted line corresponds to C_0. Inset: Average visibility of the interference fringe between the two field-2 modes. The solid line is a fit using the expression given by Eq. (3.6), with the overlap $\overline{\lambda}$ fitted to 0.95 ± 0.01.

nonclassical border in the ideal case[72] and $g_{12} \gg 2$ being the single-excitation regime for the ensembles[74].

Expressing the two-photon component for the two ensembles as $p_{11} = \xi p_c^2 \sim p_c^2/g_{12}$, we rewrite the concurrence as:

$$C \simeq \max[0, p_c(V - 2\sqrt{(1-p_c)/g_{12}})] \,, \tag{3.5}$$

where g_{12} is for either ensemble alone, with $g_{12}^{(U)} = g_{12}^{(D)} \equiv g_{12}$ assumed. The visibility V can be expressed in terms of g_{12} as the higher-order terms act as a background noise. With $(1/2)p_1p_2$ a good estimation for the background, the visibility can be written as

$$V \simeq \overline{\lambda}\,\frac{p_{12} - p_1p_2}{p_{12} + p_1p_2} = \overline{\lambda}\,\frac{g_{12} - 1}{g_{12} + 1} \,, \tag{3.6}$$

where $\overline{\lambda}$ is the overlap between fields $2_{U,D}$ (ref.[78]). In the limit of near zero excitation, as g_{12} goes to infinity, the concurrence reaches its asymptotic value given by the retrieval efficiency $\overline{\lambda}p_c$[b].

Fig. 3.3 presents our measurements of the concurrence C as a function of g_{12}. As the excitation probability is decreased, g_{12} increases as does the entanglement. The threshold to achieve $C > 0$ is found to be $g_{12}^{(0)} \simeq 7$, corresponding to a probability $p_h \simeq 1.2 \times 10^{-2}$ per trial for the creation of the heralded atomic entangled state and to a preparation rate ~ 2 kHz. Note that $C = 0$ (or C not greater than zero) does not imply that there is no entanglement, only that any possible entanglement is not detected by our protocol,

[b] An alternative approach is to determine the suppression of two-photon events relative to the square of the probability of single-photon events for the fields 2, $h \equiv \frac{p_{11}}{p_{10}p_{01}}$. $h < 1$ is a necessary condition for entanglement[27,34,36]. Here, for $g_{12} = 60$, $h = 0.060 \pm 0.005$.

which provides a lower bound for the entanglement. More importantly, in an infinite dimensional Hilbert space, entangled states are dense in the set of all states[206], so that zero entanglement is not provable for an actual experiment by way of the concurrence.

To confirm the model leading to Eq. (3.6), the inset gives the measured visibility V as a function of g_{12}. The solid line is a fit according to Eq. (3.6) with free parameter $\overline{\lambda}$, leading to an overlap $\overline{\lambda} = 0.95 \pm 0.01$, in agreement with the value $\overline{\lambda} = 0.98 \pm 0.03$ obtained from an independent two-photon interference measurement. With the fitted value of $\overline{\lambda}$ and with the independently determined value of the conditional probability $p_c = 0.135 \pm 0.005$ from measurements performed on each ensemble separately, we compare our measurements of C with the prediction of Eq. 3.5 (solid line in Fig. 3.3) and find good agreement.

Table 3.1 provides the diagonal elements of the density matrix $\tilde{\rho}_{2_U,2_D}$ and the concurrence for the case $g_{12} = 60 \pm 4$ corresponding to a probability to create atomic entanglement $p_h = 9 \times 10^{-4}$ per trial (160 Hz). A value $C = 0.092 \pm 0.002$ is directly measured at detectors D_{2a}, D_{2b} without correction. By way of the independently determined propagation and detection efficiencies, we infer the density matrix $\tilde{\rho}^{output}_{2_U,2_D}$ for fields $2_U, 2_D$ at the output of the ensembles, from which we obtain a concurrence $C^{output}_{2_U,2_D} = 0.35 \pm 0.1$. This value exceeds the then published state of the art by two orders of magnitude[27]. This leap underlines the progress obtained in terms of suppression of the two-photon component and achievable retrieval efficiency over the past year[76,77]. Finally, by way of the conditional readout efficiency $\eta = 45 \pm 10\%$ for mapping of quantum states of the U, D ensembles to the fields $2_U, 2_D$, we estimate the density matrix $\tilde{\rho}_{U,D}$ and the concurrence $C_{U,D} = 0.9 \pm 0.3$ for the collective atomic state. We emphasize that $C_{U,D}$ is an estimate determined from the model developed in ref.[74] where the fields at the output of the MOT consist of a two-mode squeezed state plus background fields in coherent states.

3.5.2 Characterization of decoherence for heralded entanglement stored in two atomic ensembles

Turning then to a characterization of the decay of entanglement with storage time τ, we present in Fig. 3.4 measurements of concurrence $C(\tau)$ for fixed excitation probability $p_h = 1.6 \times 10^{-3}$ corresponding to $g_{12} = 30$ at $\tau = 200$ ns. $C > 0$ for $\tau \lesssim 20$ μs, providing a lower bound for the lifetime of entanglement of the ensembles corresponding to 4 km propagation delay in an optical fiber.

Table 3.1: **Diagonal elements and concurrence of the density matrices for fields $2_{U,D}$, without and with correction for propagation losses and detection efficiencies.** The last column provides the estimated elements and concurrence for the atomic state by considering the readout efficiency η. $g_{12} = 60 \pm 4$.

	$\tilde{\rho}_{2_U,2_D}$	$\tilde{\rho}^{output}_{2_U,2_D}$	$\tilde{\rho}_{U,D}$
p_{00}	0.864 ± 0.001	0.54 ± 0.08	0 ± 0.3
p_{10}	$(6.47 \pm 0.02) \times 10^{-2}$	$(22 \pm 4) \times 10^{-2}$	0.5 ± 0.15
p_{01}	$(7.07 \pm 0.02) \times 10^{-2}$	$(24 \pm 4) \times 10^{-2}$	0.5 ± 0.15
p_{11}	$(2.8 \pm 0.2) \times 10^{-4}$	$(3 \pm 2) \times 10^{-3}$	0.015 ± 0.025
C	0.092 ± 0.002	0.35 ± 0.1	0.9 ± 0.3

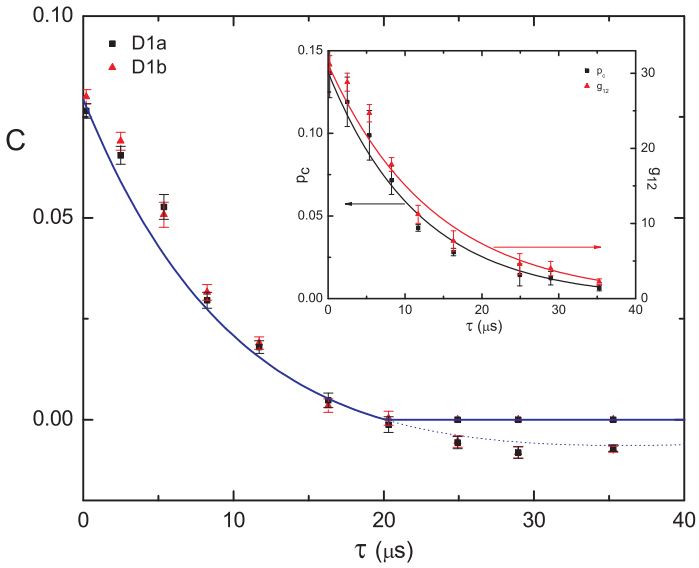

Figure 3.4: **Concurrence C as a function of the storage time τ.** The solid line is obtained from Eq. (3.5) assuming the fitted exponential decays, given in the inset, of the individual parameters p_c and g_{12} measured independently. The dotted line corresponds to C_0.

To investigate the dynamics in Fig. 3.4, the inset shows the decay of the average g_{12} and conditional probability p_c for the ensembles taken independently. Such local decoherence has been investigated as the result of inhomogeneous broadening of the Zeeman ground states due to residual magnetic fields [120,147,202]. Our current measurement shows the effect of this local decoherence on the entanglement of the joint system of the ensembles. For this purpose, our measurements of C are superposed with a line $C(\tau)$ given by Eq. 3.5, where the fitted exponential decay for $p_c(\tau), g_{12}(\tau)$ (with similar decay $\simeq$ 13 μs) and the overlap $\overline{\lambda}$ determined in Fig. 3.3 are employed. The agreement evidenced in Fig. 3.4 confirms the principal role of local dephasing in the entanglement decay.

3.6 Conclusion

In conclusion, we have reported a detailed study of the behavior of entanglement between collective excitations stored in atomic ensembles, including the dependence of the concurrence on the degree of excitation and the quantitative relationship of local decoherence to entanglement decay. The temporal dynamics reveal a finite-time decay, with separability onset for storage time $\tau_m \sim 20\ \mu s$. From a more general perspective, the inferred concurrence for the collective atomic state, $C_{U,D} = 0.9 \pm 0.3$, is comparable to then current values obtained for entanglement in the continuous variable regime [207] and for entanglement of the discrete internal states of trapped ions [197,198].

3.7 Multiple "flavors" of entanglement

While progress in traditional physics has been historically made by confirming the *consistency* of experimental data with theoretical models, it is essential to employ *robust*, *model-independent* procedures in quantum optics and quantum information science, in order to unambiguously characterize and verify the entanglement for the purported state created in one's experiment[110,208]. Diverse approaches to entanglement verification and quantification have been developed so far, including entanglement monotones and witnesses[40,110,208]. For excellent accounts of recent results, I refer to the reviews by refs.[40,208]. Also, I refer to chapters 7–9, where we have developed a particular form of an entanglement witness for verifying multipartite mode-entangled W states[38].

In this section, I would like to provide a brief overview on the different categories of entanglement[c] one could generate in an experiment, largely based on the description in ref.[110]. By this, I hope to distinguish the 'flavors' of entanglement for the *heralded* and *deterministic* quantum states described in this thesis, and those based on *post-dicted* states largely reported elsewhere in the literature (chapter 1) which are not directly applicable for scalable quantum networks[1].

1. *Deterministic* (*a priori*) entanglement

   For *deterministic* entanglement, one has a source that generates multiple copies (i.e., in de Finetti representation[211], $\hat{\rho}^{(N_c)} = \int d\hat{\rho} P(\hat{\rho}) \hat{\rho}^{\otimes N_c}$) of a state, $\hat{\rho} = \hat{\rho}_{\text{det}}$, where

   $$\hat{\rho}_{\text{det}} = \hat{\rho}_{\text{ent}}. \tag{3.7}$$

   By performing measurements on a subset of $\hat{\rho}^{(N_c)}$ (e.g., via quantum-state tomography), one concludes in principle that the physical state $\hat{\rho}_{\text{det}}$ contains an entangled state $\hat{\rho}_{\text{ent}}$ every instant of its creation. The entangled component $\hat{\rho}_{\text{ent}}$ is identical to the physical state $\hat{\rho}_{\text{det}}$ generated in an experiment. Thus, the entangled state $\hat{\rho}_{\text{ent}}$ is created on demand "at the push of the button." Importantly, the purported entanglement is unambiguously verified directly from measurements on the physical state $\hat{\rho}_{\text{det}}$ without destructively filtering a small fictitious (entangled) component $\hat{\rho}'_{\text{ent}}$ of $\hat{\rho}_{\text{det}}$ and subsequently measuring $\hat{\rho}'_{\text{ent}}$ by *post-selection* (i.e., *a posteriori* entanglement). Depending on the amount of entanglement, *deterministic* entanglement may be employed for a wide variety of large-scale quantum information tasks (section 1.1), including scalable quantum computation and entanglement distribution. For example, we demonstrated a reversible quantum interface, whereby deterministic entanglement can be mapped into and out of two quantum memories (chapter 6). Prominent examples of this type of entanglement

[c] Note that while there is only one class of entanglement (Bell states) for bipartite qubits ($N = 2$), there are different *classes* of entanglement for $N > 2$, associated with the equivalency under stochastic local operation and classical communication (SLOCC)[209,210]. My goal, however, is not to discuss about the *classes* of entanglement, which is an active research problem on its own, but rather to differentiate the various types of entanglement generated in an experiment, in terms of the amount of entanglement for the actual *physical* state.

include the various entangled states for continuous variable beams of light and atomic ensembles, and between trapped ions, Rydberg atoms, and superconducting qubits (section 1.2).

2. *Heralded* entanglement

Here, one refers to the state in the de Finetti representation $\hat{\rho}^{(N_c)} = \int d\hat{\rho} P(\hat{\rho}) \hat{\rho}^{\otimes N_c}$, where $\hat{\rho} = \hat{\rho}_{\text{her}}$ with,

$$\hat{\rho}_{\text{her}} = (1 - p_{\text{yes}}) \hat{\rho}_{\text{no}} \otimes \hat{\rho}_{\text{unent}} + p_{\text{yes}} \hat{\rho}_{\text{yes}} \otimes \hat{\rho}_{\text{ent}}. \tag{3.8}$$

This is an entangled state subject to an ensemble measurement of the subset of $\hat{\rho}^{(N_c)}$, for which one could reliably estimate the amount of entanglement $E(\hat{\rho}_{\text{ent}})$. For heralded states, we have orthogonal states $\{\hat{\rho}_{\text{no}}, \hat{\rho}_{\text{yes}}\}$ for the heralding system (*lhs* of the direct products in Eq. 3.8) with probabilities $\{1 - p_{\text{yes}}, p_{\text{yes}}\}$, for which one could subject the auxiliary states $\{\hat{\rho}_{\text{no}}, \hat{\rho}_{\text{yes}}\}$ in a test to distinguish probabilistically whether the state $\hat{\rho}_{\text{her}}$ is prepared in the entangled $\hat{\rho}_{\text{ent}}$ or unentangled states $\hat{\rho}_{\text{unent}}$. Albeit with possibly low success probability p_{yes}, we can indeed create a physical state with the desired maximally entangled $\hat{\rho}_{\text{ent}}$ with a high fidelity by projecting the ancilla states. Thus, *heralded* entanglement can be as powerful as *a priori* entanglement, except that one may have to generate many copies before obtaining $\hat{\rho}_{\text{ent}}$ if p_{yes} is small. This type of entanglement may be employed for diverse large-scale quantum information protocols, including universal quantum computations[2,212,213] and scalable quantum communications[4,9] (section 1.1).

In chapters 3–5, 8, and 9, we initially entangled the number-states between the (heralding) fields 1 and the atomic state via the two-mode squeezing operation described in chapter 2. By projecting the fields onto an entangled state $\frac{1}{2}(|10\rangle + |01\rangle)$, we prepared a high-fidelity entanglement (ideally, 1-ebit of entanglement) for the heralded state $\hat{\rho}_{\text{ent}}$ *physically stored* in the atomic ensembles. For example, in this chapter, we have achieved $C_{U,D} = 0.9 \pm 0.3$ for the physical state with $p_h \simeq 10^{-3}$ without post-selecting $\hat{\rho}_{\text{ent}}$. But as the scheme is probabilistic, the heralding process requires us to generate on average $\sim 1/p_h$ copies of the state $\hat{\rho}_{\text{her}}$ to obtain $\hat{\rho}_{\text{ent}}$. This type of entanglement can be used for conditional enhancement of entanglement distribution and connection[36,37] (chapters 4–5) and even promoted to a deterministic quantum state[79,80] via the conditional control of heralded quantum states[78], with a sufficient memory time τ_m (see ref.[115]).

3. *A posteriori* entanglement

Here, one generates $\hat{\rho}^{(N_c)} = \int d\hat{\rho} P(\hat{\rho}) \hat{\rho}^{\otimes N_c}$, where $\hat{\rho} = \hat{\rho}_{\text{post}}$ with,

$$\hat{\rho}_{\text{post}} = (1 - p_{\text{yes}}) \hat{\rho}_{\text{unent}} + p_{\text{yes}} \hat{\rho}_{\text{ent}}, \tag{3.9}$$

where $p_{\text{yes}} \ll 1$, in many cases of practical importance. Here, one devises the measurement strategy such that it is only sensitive to the desired entangled state $\hat{\rho}_{\text{ent}}$ with *post-selection*, thereby destructively

measuring the quantum state. While such a measurement strategy may display classical recording of significant non-classical correlations (e.g., by way of the violation of Bell's inequality), the actual amount of entanglement for the physical state $\hat{\rho}_{\text{post}}$ is very small: i.e., $E(\hat{\rho}_{\text{post}}) \sim p_{\text{yes}} E(\hat{\rho}_{\text{ent}})$. If the post-selection procedures can be simulated by local filters, one can in principle conclude the presence of entanglement. But, entanglement $E(\hat{\rho}_{\text{ent}})$ via post-diction greatly overestimates the amount of entanglement $E(\hat{\rho}_{\text{post}})$ in $\hat{\rho}_{\text{post}}$ (i.e., referring instead to the fictitious component $\hat{\rho}_{\text{ent}}$).

Because of the destructive nature in the measurement process, the entanglement in $\hat{\rho}_{\text{ent}}$ cannot exist independent of the null (unentangled) events $\hat{\rho}_{\text{unent}}$. Indeed, in typical downconverter experiments, with $p_{\text{yes}} \ll 1$, the quantum state one needs to assign for the two purportedly entangled optical modes is not that of a maximally entangled state $|\Psi_+\rangle = \frac{1}{\sqrt{2}}(|HV\rangle + |VH\rangle)$ of two photons, but that of a state of the form:

$$\hat{\rho}_{\text{PDC}} \simeq p_0 \hat{\rho}_0 + p_{\text{yes}} |\Psi_+\rangle\langle\Psi_+| + \hat{\rho}_{\geq 2}. \tag{3.10}$$

Thus, based on a positive detection event, one succeeds in implementing the desired protocol *a posteriori*.

Such an entangled state is not desirable for realizing most scalable quantum architectures, including quantum networks, as the amount of entanglement is extremely small for the physical state (typically, $p_{\text{yes}} \ll 10^{-3}$). Furthermore, given a density matrix $\hat{\rho}_{\text{PDC}}$, the pure-state decompositions of Eq. 3.10 may be written in a form in different pure-state decomposition, for which the pure states in the decomposition are all unentangled[178]. Unfortunately, a wide range of literature has been reported, whereby entanglement in the state of Eq. 3.10 is claimed to exist in the form of $|\Psi_+\rangle$ instead of $\hat{\rho}_{\text{PDC}}$. I refer to reference[110] for prominent examples, for which entanglement verifications were not carried out correctly.

3.8 Technical details

3.8.1 Some notes on the magic of beam displacers

The passive stability of the beam displacers has attracted us to use these components throughout our experiments (chapters 3–9). We ordered the displacers from Novaphase, for which they used laser-grade calcite crystals with exceptionally low striae and optical inhomogeneity for reducing the scattering noise of the classical beams, and polished the calcite surface with $\lambda/10$ flatness over the entire aperture and $S/D = 20/10$. However, I'd like to note that since 2009 there has been a global shortage of calcite crystals, which made them compromise the quality of calcite crystals. For example, the new batch purchased in 2010 had higher densities of scattering centers for the experiment in chapter 9, with the fluorescence clearly visible under an IR scope. As of 2011, it is unclear when we will be able to obtain high-quality calcite crystals with low scatter density as in the pre-2009 batches. Currently, for any serious quantum optics experiments involving

strong classical beam, the only practical alternative is to use synthetically grown YVO_4 beam displacers, despite the lower transmission at our wavelengths. The residual broadband fluorescence from the crystal can be overcome by employing a narrow-band high-efficiency volume Bragg grating (see Fig. 1.6 in chapter 1).